

Optical Modulation via Coupling of Distributed Semiconductor Heterojunctions in a Si-ITO-Based Subwavelength Grating


Swati Rajput^{1,*}, Vishal Kaushik¹, Prem Babu¹, Pragya Tiwari², Arvind K. Srivastava^{2,3} and Mukesh Kumar^{1,4,†}

¹*Optoelectronic Nanodevice Research Laboratory, Department of Electrical Engineering, Indian Institute of Technology Indore, Indore, India*

²*Synchrotrons Utilization Section, Raja Ramanna Centre for Advanced Technology Indore, Indore, India*

³*Homi Bhabha National Institute, Mumbai, Maharashtra, India*

⁴*Centre for Advanced Electronics, Indian Institute of Technology Indore, Indore, India*

 (Received 5 December 2020; revised 12 February 2021; accepted 1 April 2021; published 13 May 2021)

A mechanism of optical intensity modulation is proposed by utilizing the electro-optic coupling in distributed semiconductor heterojunctions of *p*-type silicon (Si) and *n*-type indium tin oxide (ITO) in the form of the subwavelength grating in a rib waveguide. The coupled multiple semiconductor heterojunctions of Si-ITO are made to exhibit efficient optical intensity modulation via electrically tunable permittivity of ITO. The subwavelength grating is a nanophotonic element that not only provides a way to couple multiple heterojunctions, but it also gives rise to efficient optical (fiber to chip) coupling at a wavelength of 1550 nm. Lateral coupling of distributed heterojunctions via depleted charge density distributed along vertical and horizontal directions enable the device to show a high extinction ratio of 24 dB. Also, electrical tuning of the coupling efficiency for an 80- μ m long device is reported, which exhibits the multifunctional nature of the proposed nanophotonic device. The proposed modulation scheme, with a modulation efficiency of 0.34 V/mm and energy consumption of 36 pJ, may open pathways for energy-efficient compact devices and circuits for large-scale optoelectronic integration. The proposed mechanism of optical modulation takes advantage of distributed semiconductor heterojunctions and enables electrically tunable inherent optical coupling with a nanophotonic element called a subwavelength grating, which further improves the modulation performance compared with a conventional Si-ITO heterojunction.

DOI: [10.1103/PhysRevApplied.15.054029](https://doi.org/10.1103/PhysRevApplied.15.054029)

I. INTRODUCTION

Silicon photonics has been exclusively reported over the past few years to unite the on-chip photonic integrated circuit and optical-interconnect applications to accomplish the ever-increasing requirement for high-speed and wide bandwidth for information processing. The prime focus of research has moved towards the linkage of integrated-circuit modules with optical-interconnect links [1–3]. By leveraging silicon (Si) photonics, momentous advances have been made in realizing low-loss optical waveguides, photodetectors, and optical modulators. Indeed, optical modulators are the most fascinating component of the optical communication system that act as a link between electrical and photonic modules [5,6]. Modulation of a propagating optical mode is obtained either by accumulation or depletion of charge carriers within the material or structure on the application of the bias, which further

undergoes a change in the complex effective index of the structure [6,7]. Notably, Si offers a compatible fabrication process, ease of chip-scale integration, strong optical confinement, and low attenuation over near-infrared wavelengths; hence, a variety of Si-based optical modulators and photonic switches employing thermo-optic and electro-optic effects have been realized to meet the demand for high-speed signal processing in data centers [7–9]. However, the weak electro-optic effect, slow tendency, and instability due to heating of the device through the thermo-optic effect, along with the absence of second-order nonlinearities in Si, lead to a larger device footprint and unwanted higher capacitances [4–10]. In the last few years, many evolutions, in terms of hybridizing Si or designing engineered structures, have occurred to overcome the intrinsic constraints of Si-based optical modulators [10–12]. The main aim of this modification is to achieve a breakthrough in the modulator's performance in terms of footprint, speed, and energy efficiency. Incorporating a Si-based optical modulator along with a high-quality factor-resonating structure can enhance modulation efficiency,

*rajput.swati18692@gmail.com

†mukesh.kr@iiti.ac.in

but endures a shortened bandwidth with thermal instabilities [11–16]. Simultaneously, Si-based plasmonic modulators are quite popular due to their high-field confinement, which enlarges the electro-optic coefficient, but plasmonic modulators increase the high intrinsic loss due to the metallic layer [17–19].

Further graphene-based optical modulators are reported to exhibit strong modulation efficiency by electrically manipulating the Fermi level of graphene; these modulators lead to difficulties in fabrication and in achieving good optical confinement in an atomically thin layer [20–22].

The issue of the poor electro-optic effect in Si can be resolved by introducing the concept of hybrid modulators i.e., adding an electro-optic material to the Si structure [23–26]. The electro-optic material can be an organic thin film or epsilon-near-zero (ENZ) materials; however, organic thin-film modulators can further add to electrical instabilities. At times, the ENZ materials, especially transparent conducting oxides (TCOs), prove to be promising for highly efficient optical modulation [27–29]. Among TCOs, indium tin oxide (ITO) is a potential electro-optic material due to its electrically tunable permittivity, near-infrared wavelength, and good compatibility when integrated into the Si structure [30–32]. ITO is an *n*-type wide-band-gap semiconductor, the optical characteristics of which can be electrically tuned by adjusting the electron concentration. By either electron accumulation or depletion in ITO, the permittivity can be varied from a positive value to a negative value across the telecommunication window. While tuning the permittivity of ITO, there is a regime where permittivity reaches close to zero; this regime is called the ENZ regime [15,23,32,33]. This ENZ condition is a state of the art where there is a sudden change in the absorption of ITO, which opens gateways for realizing intensity or electroabsorptive modulation by amalgamating ITO with the Si structure [29,31,34,35].

In integrated photonic devices, including on-chip optical modulators, in coupling from fiber to chip and out coupling from chip to fiber leads to another complication.

Usually, fiber couplers are utilized for optical guidance in a modulator, but they still suffer from submicron-incorrect positioning and need additional edge polishing [36–38]. To improve the compactness and commercial yield of an optical modulator, resonating or periodic grating structures can be appended to the waveguide, which increases the light-matter interaction [13,14]. Subwavelength-grating (SWG) waveguide technology provides a platform with which to accomplish high performance, compact, and cost-effective on-chip photonic devices for optical-interconnect and quantum-photonics applications [39–42]. The SWG coupler exhibits an efficient optical coupling efficiency and eliminates the need for additional edge polishing for end-fire coupling.

Here, a mechanism for optical modulation is demonstrated on SOI substrate, utilizing the electro-optic

coupling in distributed semiconductor heterojunctions of *p*-type Si and *n*-type ITO in the form of a subwavelength grating in a rib waveguide. The subwavelength grating is a nanophotonic element that furnishes a way to couple multiple semiconductor heterojunctions and enables efficient optical (fiber to chip) coupling at a wavelength of 1550 nm. The coupling of silicon-ITO-based multiple heterojunctions is utilized to enable efficient intensity modulation and electrically tunable coupling efficiency. Unlike traditionally employed optical modulation, the proposed nanophotonic scheme benefits from the optical modulation-cum-coupling obtained with an optimized high-index contrast grating in the form of multiple Si-ITO heterojunctions that employ the ENZ state of ITO for electrical control of the optical characteristics. The proposed mechanism is conceptualized in such a manner to attain efficient intensity modulation with an in-built functionality of fiber-chip coupling without any requirement for extra input and output grating couplers. The hybrid structure is designed effectively to achieve strong optical confinement in a high-index contrast subwavelength grating, which provides input and output coupling, as well as playing the role of Si-ITO heterojunctions distributed such that the propagating optical beam can be controlled by the electrically tunable permittivity of ITO and added to the intensity modulation of the guided light at 1550 nm wavelength. The distributed Si-ITO heterojunctions here refer to horizontal heterojunctions across Si-ITO subwavelength gratings and vertical heterojunctions across Si or ITO in the grating region with ITO or Si layers on the top and bottom, respectively. The depleted charge-carrier density across multiple heterojunctions is laterally coupled, which together with the ENZ state of ITO electrically tune the coupled power and modulate the intensity of the propagation beam effectively. We experimentally demonstrate a potent mechanism for a compact intensity modulator with an on-off extinction ratio of 24 dB for an 80- μm -long device driven by a favorably small reverse bias of -4 V. Theoretical analysis of the subwavelength-grating coupler efficiency and modulation characteristics is done by employing the well-established optical and electrical modeling tool LUMERICAL. Analysis of the ITO charge-carrier concentration is done to study the modulator's incorporation of the ENZ effect. The distributed Si-ITO heterojunction in a grating coupler in the rib waveguide is fabricated on *p*-doped SOI wafer by using electron-beam lithography followed by reactive-ion etching, and further ITO is deposited on the patterned and etched structure by employing ion-assisted *e*-beam system.

In our previously reported work [23], we experimentally demonstrated a hybrid optical modulator as a conventional Si-ITO heterojunction and observed an extinction ratio of 7 dB for a 1.7-mm-long device at a maximum reverse bias of -5 V. However, the device struggles with a low extinction ratio and larger device footprint, as the real active area, i.e., the junction, is small with respect to the total

mode area; in other words, the interaction of light with the active region is very limited. Introducing electro-optic coupling into distributed semiconductor heterojunctions in a Si-ITO-based subwavelength grating in a rib waveguide increases the light-matter interaction and the electrically tunable in-built optical coupling will further add to a high extinction ratio and smaller device footprint. The approach in the present mechanism of optical modulation is to engineer the structure to maximize the interaction of light with the active region i.e., the Si-ITO heterojunction of the structure. To achieve the same, the surface is provided with periodic perturbations in the form of a grating, where materials (Si-ITO) are not only overlapping vertically but also horizontally to form junctions. The proposed twofold beneficial structure i.e., intensity modulation with an in-built functionality of coupling, will allow scope for broad-band optical communication and quantum computing. The low energy consumption and footprint of the proposed device will undoubtedly enable cost-effective large-scale photonic integration.

II. PROPOSED MECHANISM

The mechanism of optical-intensity modulation with in-built coupling to utilize electro-optic coupling in distributed semiconductor heterojunctions of p -type Si and n -type ITO in the form of a subwavelength grating in a rib waveguide is presented for operation at a wavelength of 1550 nm. The perspective of the proposed mechanism is to efficiently couple light in a Si (p -type)-ITO (n -type) subwavelength-grating-based rib waveguide and utilize the lateral electro-optic coupling of p - n heterojunctions in the

gratings to electrically tune the permittivity of ITO, which further improves the coupling efficiency and modulates the intensity of the propagating optical beam with respect to reverse bias. A schematic representation of the proposed nanophotonic scheme with twofold benefits i.e., optical modulation with in-built coupling, is shown in Fig. 1(a). The proposed structure is designed to be fabricated on a highly doped p -type SOI wafer with a Si layer on the top with a thickness of 220 nm. A single-layer uniform periodic one-dimensional grating of high-index ($n = 3.48$) Si surrounded by an alternating layer of low-index ($n = 1.3$) ITO is formed. The high-index contrast subwavelength grating in the form of a rib waveguide is the nanophotonic element that provides leverage for in coupling, i.e., fiber to chip, and out coupling, i.e., chip to fiber, and plays the role of a heterojunction as well. The grating parameters of the coupler are assiduously amended for efficient coupling with a low loss at 1550 nm. The optimal grating parameters are calculated to be the grating period ($\Lambda = 600$ nm) with 50% duty cycle, grating height ($h = 130$ nm), and grating length, i.e., rib width of $5 \mu\text{m}$. To bring about good overlap of the optical mode, an ITO of thickness of 50 nm is arranged on the top of Si-ITO grating.

To acquire a proficient modulation efficiency and adequate region of the ENZ effect, an increase in the electron concentration of ITO is achieved by varying the oxygen partial pressure during the deposition of ITO on the SOI wafer. Different oxygen partial pressures during deposition produce defect interstices, giving rise to charge density. Room-temperature Hall effect measurements are done to find the type of conductivity and charge density. The optical constants of the ITO thin films deposited at

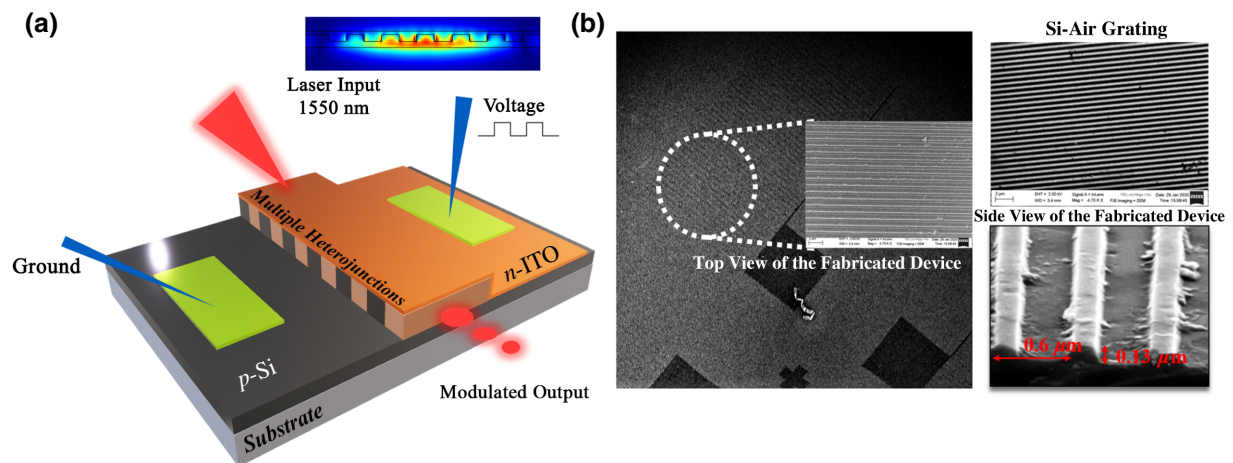


FIG. 1. Schematic of the proposed scheme of optical-intensity modulation and microscopic images of the fabricated device. (a) Design of Si (p -type)-ITO (n -type) multiple-heterojunction-based subwavelength gratings in a rib waveguide on SOI wafer to couple free-space light and modulate the complex effective index of the propagating optical beam at 1550 nm. Proposed nanophotonic structure is fabricated on SOI wafer, where grating period (Λ) is 600 nm with a height of 130 nm and grating length (rib width) of $5 \mu\text{m}$. Thickness of ITO on top of the Si-ITO grating is 50 nm. Inset on top of the device depicts field propagation in laterally coupled multiple-heterojunction-based grating coupler. (b) Scanning electron microscope outlook of the top surface and side view of the fabricated device along with the patterned Si-air grating.

distinct oxygen partial pressures are calculated using an ellipsometer. For all three films, ellipsometry measurements with respect to bias are performed on ITO thin films exhibiting the ENZ state. Furthermore, the nanophotonic structure is fabricated by using standard nanofabrication facilities. The coupling and modulation characteristics of the fabricated structure are investigated using an optical characterization setup without an additional input and output grating coupler. The device does not work as a conventional grating coupler that feeds into another waveguide, but rather it acts as a waveguide with an in-built coupler.

III. ANALYSIS OF COUPLING OF DISTRIBUTED SEMICONDUCTORS HETEROJUNCTIONS

The light-matter interaction with junctions in the proposed work is magnified by introducing multiple

heterojunctions into the grating. The structure is provided with periodic perturbations in the form of the grating, where Si-ITO not only overlaps vertically but also horizontally forming junctions. In the structure specifically, two types of laterally coupled distributed semiconductor heterojunction i.e., horizontal heterojunctions and vertical heterojunctions, lead to enhanced carrier depletion across the junction for efficient modulation characteristics with respect to reverse bias. The horizontal heterojunction is basically formed laterally across the grating of *p*-Si and *n*-ITO, whereas the vertical heterojunction is formed laterally across *p*-Si in the grating domain and ITO layer on the top of the subwavelength gratings, as displayed in Fig. 2(b).

On the application of the reverse bias, the lateral coupling of depleted charge density across the distributed

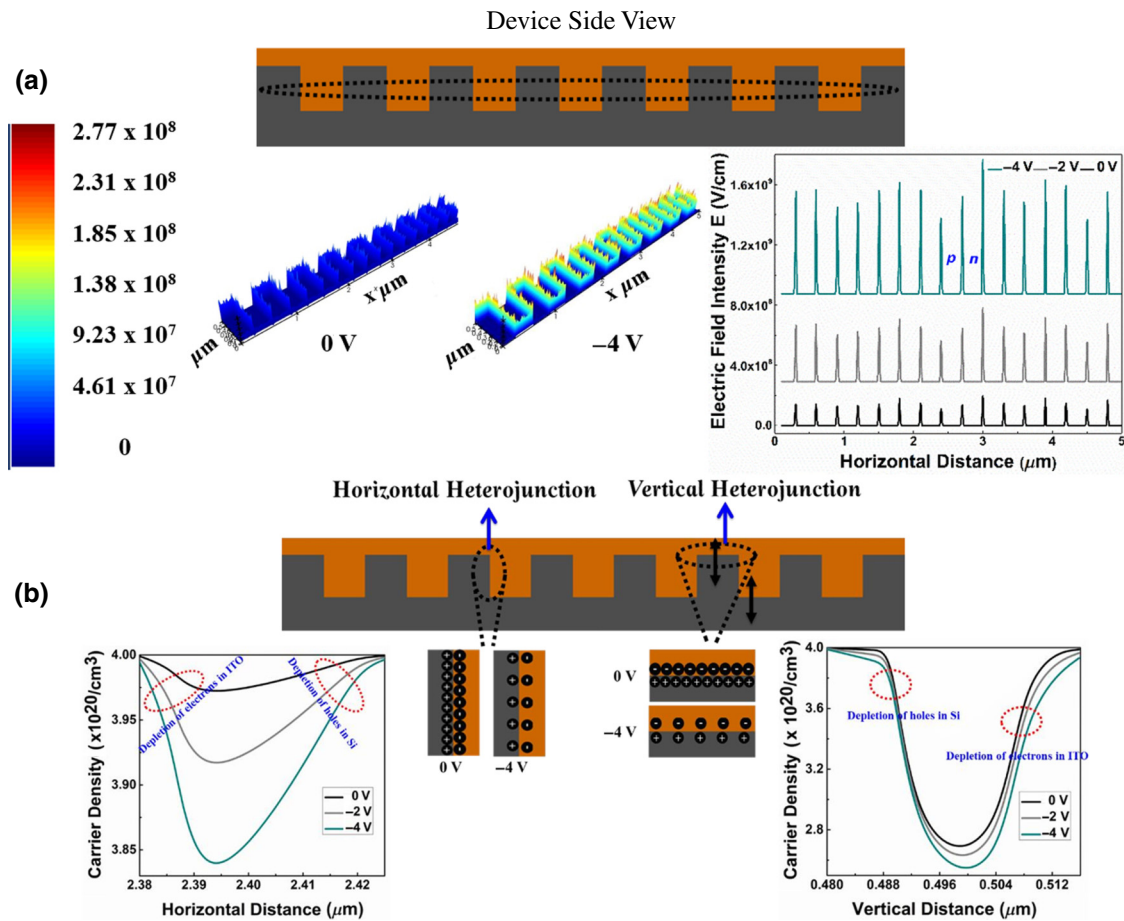


FIG. 2. Illustrative view of device operational concept and distributed Si-ITO heterojunctions, i.e., horizontal and vertical heterojunction configurations embedded in the subwavelength-grating-based rib structure. (a) Three-dimensional view of enhanced electric field along the direction of propagation of Si-ITO subwavelength gratings in on and off states, respectively. Right-hand plot in (a) is the electric field intensity averaged along the vertical heterojunction. Sudden rise in electric field signifies widening of the depletion region, which essentially changes the charge-carrier profile. (b) Computed charge-carrier profile with respect to reverse bias, specifying a separate concentration of electrons and holes with the help of an inset, exhibiting horizontal and vertical heterojunctions. Carrier profiles in horizontally and vertically aligned heterojunctions are different, probably owing to different electric field distributions in both sets of interfaces. Majority of charge carriers in Si and ITO are holes and electrons, respectively, and clearly specified with the position of the Si-ITO interface.

semiconductor heterojunctions productively tunes the permittivity of ITO to the ENZ region. Altogether, the near-zero permittivity of ITO modulates the intensity remarkably and converts the passive coupler into an active one.

In absence of any bias, both p -Si and n -ITO have a charge density of $4 \times 10^{20}/\text{cm}^3$. On application of the reverse-bias voltage across the structure, the charge carriers across vertical and horizontal heterojunctions start to become depleted; hence, with increasing bias, widening of the depletion width accompanied by a high field intensity across both junctions is observed. Figure 2(a) exhibits a three-dimensional view of the enhanced electric field along the direction of propagation of Si-ITO subwavelength gratings in the on and off states, respectively.

The right-hand plot in Fig. 2(a) is the electric field intensity averaged along the vertical heterojunction. The sudden rise in electric field signifies widening of the depletion region, which essentially changes the charge carrier profile. Figure 2(b) exhibits the depletion of electrons and holes across individual vertical and horizontal heterojunctions with respect to reverse bias.

Figure 2(b) clearly specifies the Si-ITO interface positions. The charge-carrier profiles denote separate concentrations of electrons and holes with the help of an inset. The majority of carriers in Si and ITO are holes and electrons, respectively, and with the position of the Si-ITO interface clearly specified, it can be safely assumed that the contribution from minority charge carriers on each side can be neglected. This allows us to plot electron and hole concentrations in the same graph, providing the junction position is clearly specified. Also, since the carrier profiles in horizontally and vertically aligned heterojunctions are different, owing to different electric field distributions, two separate graphs are required to show the change in carrier profile at both sets of interfaces. Likewise, several of such distributed semiconductor heterojunctions are laterally coupled to attain a high depletion density, enhanced field, and light-matter interaction. The light-matter interaction increases due to the enhancement of the effective tunable area by increasing the junction area where carriers can be tuned.

Although carrier accumulation, i.e., the p - i - n structure, shows a greater change in permittivity, giving rise to changes in the modal effective index, compared with carrier depletion, i.e., the p - n junction structure, the p - n junction structure is still more widely adopted than the p - i - n structure due to the higher-speed performance of the former. The speed performance of the p - i - n structure is hindered by a sluggish carrier-diffusion time and lifetime.

IV. MATERIAL PROCESSING AND DEVICE FABRICATION

To experimentally verify the strong electro-optic effects in ITO using the ENZ effect, ITO is deposited on p -type

SOI wafer at three distinct oxygen partial pressures. Depositing ITO at various oxygen partial pressures will yield different electron densities in the ITO layer. The optical constants of the ITO layer can be electrically tuned by variation of its electron charge density. When the electron charge density of the ITO layer is optimized at a zone where its permittivity is close to zero, i.e., the ENZ state, a larger change in the attenuation of ITO can be seen, making it a potential candidate for intensity modulation at 1550 nm with a larger modulation efficiency. ITO acts as a free-electron Drude material, the optical attributes of which are monitored by its motile electron concentration.

The optical permittivity of ITO is given by

$$\varepsilon_{\text{ITO}} = \varepsilon_{\infty} \frac{\omega_p^2}{\omega^2 + i\omega\Gamma}, \quad \omega_p^2 = \frac{N_e^2}{\varepsilon_0 m_{ce}^*},$$

where ε_{∞} is the background dielectric constant, ω is the angular frequency of light, and Γ is the collision frequency of the electrons in the ITO layer. The plasma frequency, ω_p , of ITO revolves around the electron charge density, N_e ; electron charge magnitude, e ; vacuum permittivity, ε_0 ; and the electron's effective mass, m^* . The electron charge density can be passively altered via annealing or actively altered through the applied electric field.

To attain optimal modulation efficiency, the optical properties of the ITO layer deposited on highly doped p -type SOI wafer at three distinct oxygen partial pressures, i.e., (i) 1 sccm O_2 and 30 sccm Ar, (ii) 0.5 sccm O_2 and 30 sccm Ar, and (iii) 0 sccm O_2 and 30 sccm Ar, are examined. The deposited ITO thin films represented in Fig. 3(a) exhibit n -type conductivity and the carrier densities are measured to be $0.89 \times 10^{20}/\text{cm}^3$ (ITO deposited at 1 sccm O_2), $2.87 \times 10^{20}/\text{cm}^3$ (ITO deposited at 0.5 sccm O_2), and $4.76 \times 10^{20}/\text{cm}^3$ (ITO deposited at 0 sccm O_2).

The ITO layer deposited at 0 sccm O_2 seems to be more conductive because of the presence of defect states, but as the flow of oxygen increases, the vacancies are filled by oxygen atoms, leading to reduced defect states contributing to lower conductivity [23,43–48].

Ellipsometry measurements are done on the three ITO deposited wafers to calculate the real part of permittivity. The real part of permittivity for different electron concentrations is shown in Fig. 3(c). The real part of permittivity decreases steadily with increasing wavelength towards the infrared region. At some wavelength, the permittivity reaches to very close to zero; this point is defined as the ENZ state. Figure 3(c) reveals that the ITO layer, with a concentration of $4.87 \times 10^{20}/\text{cm}^3$, has a positive permittivity of real $\varepsilon_{\text{ITO}}=0.8$ at 1550 nm. When the real part of the permittivity comes close to zero, there is a dramatic alteration in the real and imaginary parts of the refractive index of ITO. Hence, on the ITO-coated SOI wafer with a carrier concentration of $4.87 \times 10^{20}/\text{cm}^3$, the real and imaginary parts of the refractive index, with respect to

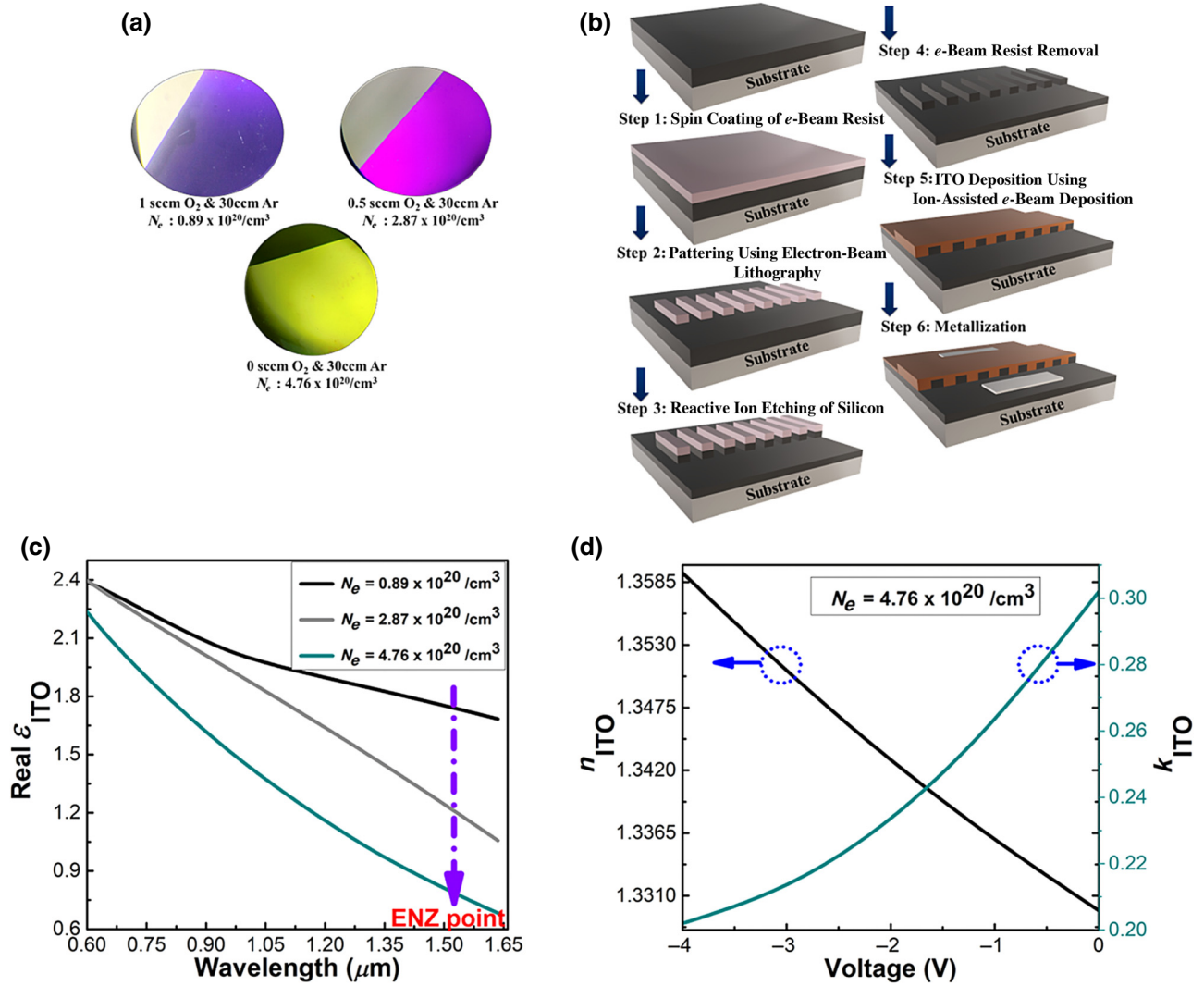


FIG. 3. (a) Visual appearance of ITO deposited on SOI wafer at various oxygen partial pressures. (b) Schematic of the standard fabrication process of the prospective structure on *p*-doped SOI wafer. (c) ITO characterization, i.e., ellipsometry measurement, to study the modulation mechanism in ITO using the ENZ effect. Real part of the Drude model permittivity with respect to wavelength for ITO thin films with different electron concentrations realized by adjusting the oxygen partial pressure during deposition followed by postannealing procedure. Drude parameters are extracted by fitting variable-angle spectroscopic ellipsometric (VASE) data from ellipsometry measurements using the ITO general-oscillator model. Violet arrow denotes the ENZ region and decrease in the real part of permittivity (coming close to ENZ point) with increasing carrier concentration. (d) Variation in real and imaginary parts with respect to voltage of ITO thin film exhibiting ENZ state with a carrier concentration of $4.76 \times 10^{20} / \text{cm}^3$.

reverse-bias voltage, are measured, as shown in Fig. 3(d). With an increase in the reverse bias, the real part of the refractive index of ITO increases, and the imaginary part of the effective index decreases tremendously. This decrease in the imaginary part (attenuation coefficient) of ITO's refractive index will affect the effective index of mode overlap in multiple Si-ITO heterojunctions to attain a higher modulation strength. Spectroscopic ellipsometry is a point-contact optical technique to measure the optical constants of a material with high accuracy. The change in the imaginary part of ITO in the planar substrate is 0.1, which is measured at a single point. After the optimization

of ITO's electron charge density for a strong modulation strength, fabrication of the grating-coupler-based rib structure is done by following the standard fabrication process presented in Fig. 3(b). The scanning electron microscope (SEM) images of the top and side views of the fabricated structure on SOI wafer and top surface of the Si-air grating are depicted in Fig. 1(b).

V. MODULATION AND COUPLING CHARACTERISTICS

The depleted charge concentration across the distributed Si-ITO heterojunctions tunes the optical constant, i.e.,

refractive index (permittivity) of ITO, validating the ENZ effect at 1550 nm in unison with the Drude model. The electrically tunable permittivity of ITO makes the modal effective index of the grating coupler voltage dependent. The depletion of charge-carrier density across vertical and horizontal heterojunctions will remarkably affect the permittivity of ITO. Furthermore, variation in the permittivity will efficiently affect the modal-complex effective index given by [7,8,23]

$$\Delta n = \frac{-e^2 \lambda^2}{8\pi^2 c^2 \epsilon_0 n} \left(\frac{N_e}{m_{ce}^*} + \frac{N_h}{m_{ch}^*} \right), \quad (1)$$

and

$$\Delta \alpha = \frac{e^3 \lambda^2}{4\pi^2 c^3 \epsilon_0 n} \left[\frac{N_e}{\mu_e (m_{ce}^*)^2} + \frac{N_h}{\mu_h (m_{ch}^*)^2} \right], \quad (2)$$

where N_e and N_h are electron and hole concentrations, respectively; e is the electronic charge, μ_e and μ_h are the mobilities of electron and hole, respectively; and m_{ce}^* and m_{ch}^* are the effective masses of electron and hole,

respectively. Figure 4(a) exhibits the two-dimensional mode profile for both on and off states.

For a maximum reverse bias of -4 V, the variation in the real part of the effective index (Δn_{eff}) observed is 9×10^{-3} and the variation in the imaginary part of the effective index, Δk_{eff} , is 1.15×10^{-2} at 1550 nm wavelength.

With increasing reverse bias, there is an increase in the real part and a decrease in the imaginary part of the effective index, as shown in Fig. 4(b). The real part implies the phase velocity, whereas the imaginary part implies the attenuation coefficient of the propagating beam. Consequently, because of variation in the real part, the phase velocity is triggered, which evidently changes the coupled power in the device with respect to the voltage, as displayed in Fig. 4(c). The phase velocity plays the main role in strong optical confinement within the structure, which leads to enhancement in the coupling efficiency from 34% to 66% with increasing reverse bias. The coupled power is measured using $P_{\text{coupled}} = P_{\text{injected}} - (P_{\text{reflected}} + P_{\text{transmission}})$. Power transmission monitors are placed below and above the Si-ITO heterojunction-based grating coupler to measure the reflected and transmitted power, which is later subtracted from the injected power.

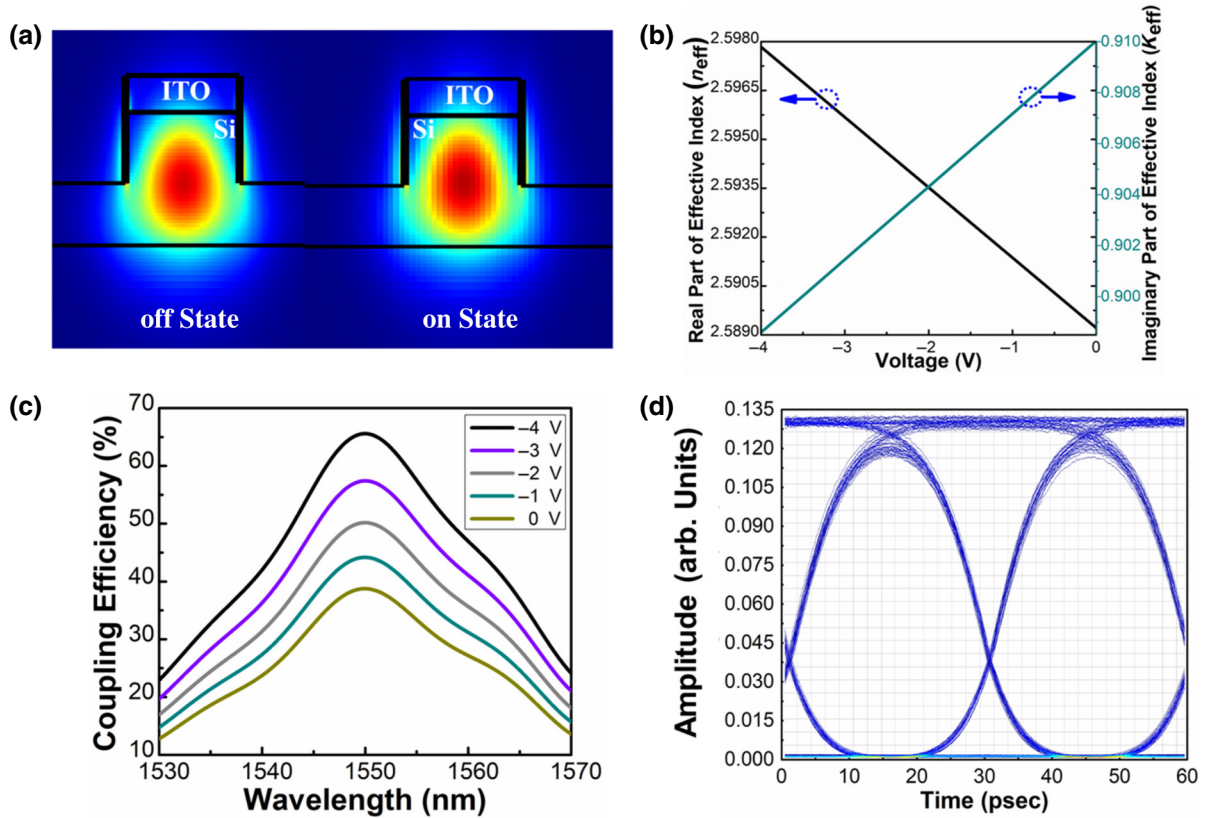


FIG. 4. (a) Two-dimensional modal field profile with scale bar of the proposed device in off and on states with an applied reverse bias at 1550 nm wavelength. (b) Computed numerical plot of real and imaginary parts of the effective index of the propagating optical beam, with respect to reverse-bias voltage; (c) theoretically calculated coupling efficiency with respect to wavelengths ranging from 1530 to 1570 nm at different reverse-bias voltages; and (d) simulated diagram for output signal modulated at 35 Gbit/s.

P_{injected} is basically the optical power injected at the input end of the device, i.e., modulator-cum-grating coupler, and P_{coupled} is the coupled power from the output end of the device. For complete simulation details, please refer to the numerical analysis section. The change in coupling efficiency is also attributed to an increase in the contrast of the refractive index of Si and ITO. As shown in Fig. 3(d), when a reverse bias is applied, ITO's real part of the refractive index decreases; hence, when a reverse bias is applied in the waveguide, depletion across the junction changes ITO's refractive index. This decrease in refractive index increases the refractive-index contrast between Si and ITO. Hence, the change in coupling efficiency by 30% is because of both the material's property and waveguiding. Alteration of the phase owing to variation in the real part of the effective index is given as [6–8] $\Delta\phi = 2\pi \Delta n_{\text{eff}} L_{\pi} / \lambda$, where L_{π} is the phase-shifter length for 180° transition of the beam.

In the present structure, $\Delta n_{\text{eff}} = 9 \times 10^{-3}$, and hence, to attain 180° transition, the device length required is $86 \mu\text{m}$. The attenuation coefficient of the propagating optical beam is given by [9] $ER = 4.343[\alpha(0) - \alpha(V)]L$. For the structure of $85 \mu\text{m}$ in length and a maximum bias of -4 V , an extinction ratio of 26.15 dB is calculated. Computational results suggest that the proposed nanophotonic scheme shows twofold benefits, i.e., an optical modulator exhibiting a high extinction ratio with an in-built functionality of an electrically tunable coupler. The device displays a junction capacitance of 4.56 pF, hence the RC -limited bandwidth [6–8], $1/2\pi RC$, is calculated to be 34.85 GHz, where R is 90Ω . This results in a small dynamic energy [6–8], $1/CV^2$ of 36.54 pJ. Figure 4(d) depicts an output modulated signal at 35 Gbit/s. A non-return-to-zero (NRZ) voltage signal

with a pseudorandom bit sequence (PRBS) and a bit rate of 35 Gbit/s is applied to the modulator in LUMERICAL INTERCONNECT.

Since the tuning of ITO also impacts on the coupling efficiency, the device is characterized to assess if the contribution from the change in coupling efficiency has a constructive or destructive effect on the overall modulation performance. Figure 4(c) shows the theoretical coupling efficiency of the coupler, which can be seen to increase with the negative bias voltage, and the maximum and minimum coupling efficiencies achieved are at -4 and 0 V , which correspond to the device on and off states, respectively. It can thus be concluded that the change in coupling efficiency, as well as modulation of the device, is working in tandem, where both are shown to individually increase the attenuation at 0 V and improve the transmission at -4 V .

Thus, the nanophotonic structure proves to be compact, cost effective, and energy efficient due to the small device footprint, absence of an additional input-output coupler, and lower-energy consumption. Despite changes in both the real and imaginary parts of the effective index, the change in the imaginary part outweighs the change in the real part; hence, we find that the device is better for intensity modulation than the phase shifter. We experimentally realize the structure to study the intensity-modulation characteristics.

VI. OPTOELECTRONICS MEASUREMENTS

An illustrative representation of the optoelectronic measurement setup is presented in Fig. 5(a), along with a

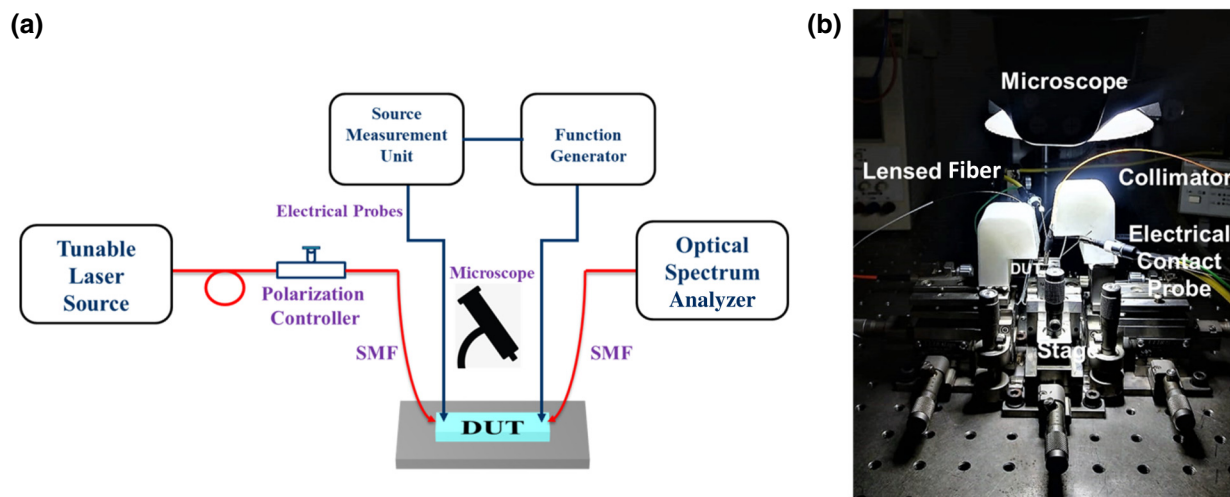


FIG. 5. (a) Illustrative representation of experimental optoelectronic characterization setup composed of tunable laser source, polarization controller, high-resolution optical-spectrum-analyzer, single-mode lensed fiber (SMF), vacuum stage, device under test (DUT), source measurement unit, function generator, and optical microscope. (b) Photograph of electrical and fiber-optic probe station used for device measurements.

photograph of the fiber and electrical probes used to characterize the device in Fig. 5(b). The setup is composed of a laser source of wavelength 1527–1566 nm, a polarization controller, a microscope, and a high-resolution optical spectrum analyzer. The fiber-optic output from the laser source excites the TE-polarized mode at the input of the device under test, i.e., Si-ITO multiple-heterojunction-based grating coupler in a rib waveguide. Transmitted light at the other end of the device is collected via a single-mode lensed fiber. To measure the maximum coupled power, the input and output single-mode lensed fiber is aligned at 0° , 5° , and 10° with respect to the normal of the surface of the device under test. The electrical probe arms are placed on the contacts very precisely using an optical microscope. These probe arms are connected to the source measurement unit via BNC cables.

Figure 6(a) represents the experimentally measured transmission spectrum of the fabricated grating coupler at different angles of incidence, i.e., 0° , 5° , and 10° , with respect to the grating normal. The output power is normalized to the input power and plotted in dB. With increasing angle of incidence, the transmission of the propagating

optical beam from the laser source increases. A maximum transmission of -26.84 dB is calculated at 1552 nm for a 10° angle of incidence from the grating normal. Comparing the performance of the proposed Si-ITO grating coupler with state-of-the-art external couplers, the introduction of ITO influences the performance of the coupler, as the refractive-index contrast in the Si-ITO grating coupler is compromised when compared with the Si-air grating coupler. At the same time, ITO provides the necessary electrical tunability to the proposed grating-based design. Although the device insertion loss of -7 dB is relatively high, if compared with state-of-the-art external couplers, extra functionality of electrically tunable coupling efficiency with a moderate insertion loss of the device makes it unique. The choice of device geometry is such that, on one hand, it improves the light-matter interaction for better modulation efficiency and, on the other hand, its inherit grating-type structure allows coupling of free-space light to the waveguide mode.

On applying the reverse-bias voltage on the fabricated device, the depletion of charge carriers across Si-ITO multiple heterojunctions leads to variation in the complex

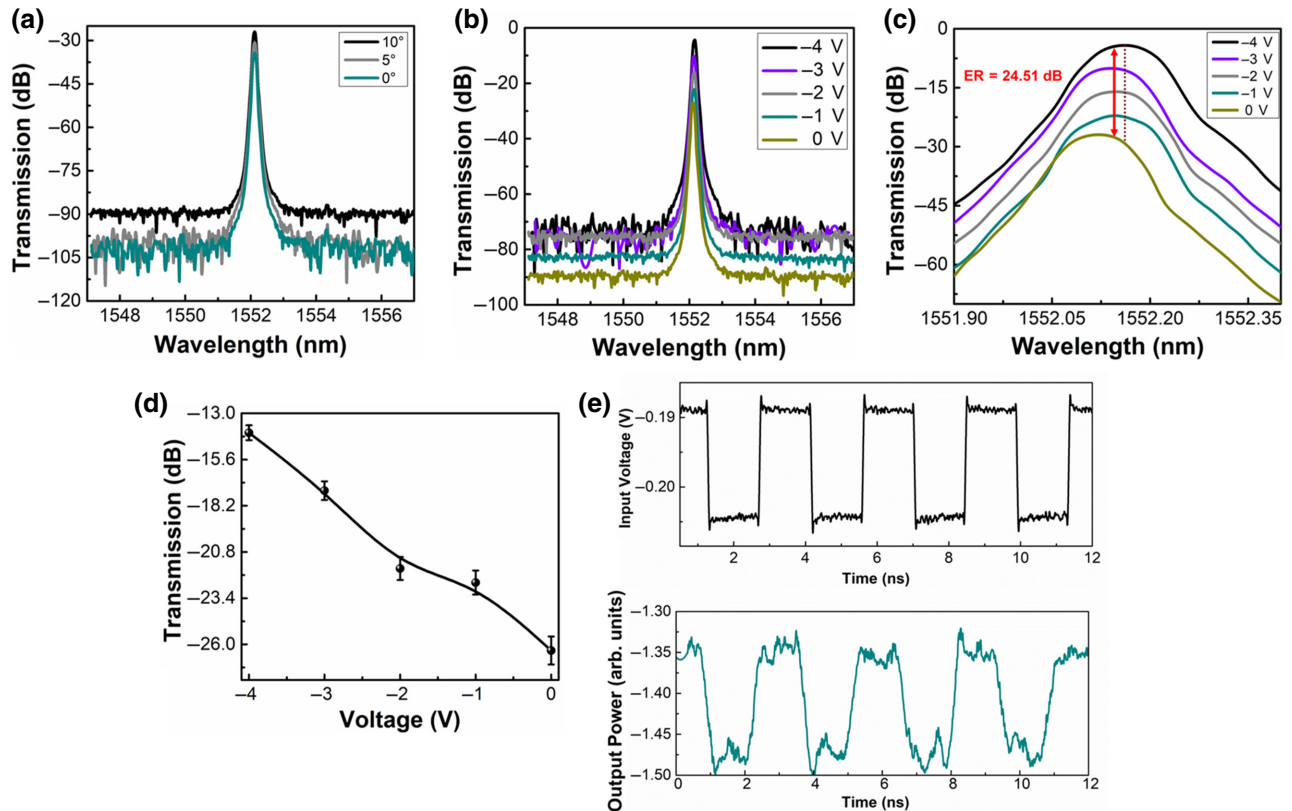


FIG. 6. (a) Experimentally measured transmission spectrum of fabricated subwavelength-grating coupler at different angles of incidence with respect to grating normal. (b) Experimentally measured transmission spectrum with increasing reverse-bias voltage. (c) Extinction ratio calculated from transmission spectrum. (d) Experimental fitting of transmission versus voltage at a fixed wavelength of 1552 nm for different sets of measurements on five sets of devices. Percentage error may be because of fiber misalignment or fabrication tolerance. (e) Time-domain analysis to show dynamic response of the modulator with a pulse frequency of 300 MHz.

TABLE I. Comparison of the performance of the proposed device with state-of-the-art devices in terms of ER and linear device footprint.

Material	Device type	Linear footprint (μm)	ER (dB)
Lithium niobate (LiNbO_3) [49]	Mach-Zehnder modulator	7000	8
Si [50]	Mach-Zehnder modulator	3000	3
ENZ-Si [25]	ITO- HfO_2 -silicon metal-oxide-semiconductor (MOS) capacitor with ITO	1	0.1
Graphene [20]	Monolayer graphene on Si bus waveguide	1	0.1
Graphene [51]	Double-layer graphene on Si bus waveguide	1	0.16
ITO [23]	Hybrid waveguide based on Si-ITO heterojunction	1000	7
ITO [this work]	Multiple Si-ITO heterojunctions based subwavelength grating in a rib waveguide	80	24
Si [52]	Hybrid plasmonic waveguide	1	1

modal effective index of the propagating optical beam at an alignment of 10° for the single-mode lensed fiber. The voltage-induced change in the complex effective index changes the intensity of the propagating beam with respect to the reverse bias, in accordance with the ENZ effect and the Drude model of ITO. Figure 6(b) exhibits the transmission spectrum at different reverse-bias voltages, where output power is normalized to input power. The maximum and minimum output powers achieved are -7 and -31 dB, respectively.

The transmission from the fabricated device increases with an increase in the reverse bias due to a decrease in attenuation, i.e., the imaginary part of the effective index. Figure 6(c) shows the experimental extinction ratio calculated from the transmission spectrum at different reverse-bias voltages. The extinction ratio calculated is 24.51 dB for a maximum voltage of -4 V and device length of $80 \mu\text{m}$. Figure 6(d) depicts the experimental fitting of transmission versus voltage at a fixed wavelength of 1552 nm for a different set of measurements on five different samples. The percentage error may be because of fiber misalignment or fabrication tolerance.

Time-domain analysis is conducted to estimate the device speed. A continuous laser light beam is coupled to the device under test and a high-speed pulse wave form is provided to the device with 50% duty cycle. The optical output of the device is then recorded with the help of a photodetector, the photocurrent of which is recorded with the help of small resistance and a digital storage oscilloscope (DSO). The voltage difference across the resistance is directly related to the current in the circuit by $V=IR$. The current in the circuit is dictated by the response of the photodetector, as the value of resistance chosen is very small. As the output optical power of the modulator changes, the change in photocurrent is reflected by the voltage drop across the resistance and is finally recorded using a DSO. The contrast in Fig. 6(e) thus actually reflects the voltage drop across the resistance. Figure 6(e) shows the dynamic response of the modulator with a pulse frequency of 300 MHz for estimating the rise and fall time

of the device and it is represented in arbitrary units. Transient analysis shows a rise time and fall time of around 0.12 ns, from which the modulation speed of the device can be estimated to be around 8 GHz. Table I exhibits a comparison of the proposed intensity modulator with state-of-the-art modulator in terms of extinction ratio (ER) and linear device footprint. The demonstrated modulation scheme depicts a competitive extinction ratio and smaller device footprint. Hence, the reported multiple Si-ITO heterojunction based optical modulation scheme with in-built coupling represents a practical option to other, less-well performing, Si and LiNbO_3 state-of-the-art optical modulators, without necessitating the use of external grating couplers.

Thus, undoubtedly, the main fascination of the proposed scheme is its dual functionality, i.e., optical modulator with an in-built coupler. The proposed concept of the device function enables inherent optical coupling, which can be tuned electrically. Besides this, the proposed structure can also act as an on-chip passive coupler. A high extinction ratio compact intensity modulator based on laterally electro-optically coupled distributed semiconductor heterojunctions can also be utilized as a Mach-Zehnder interferometer-based phase shifter. Furthermore, the high-order nonlinearities of ITO near the ENZ region can open avenues to realize and study exotic nonlinear effects for developing more proficient optical modulators.

VII. CONCLUSIONS

We conceptualize the device by hybridizing silicon with ITO in the form of a subwavelength grating consisting of distributed semiconductor heterojunctions to provide optical-intensity modulation. A mechanism for optical modulation with in-built functionality of coupling based on the electro-optical coupling of distributed semiconductor heterojunctions in Si-ITO subwavelength gratings is proposed. The subwavelength grating is the nanophotonic element in the structure that is optimized

to exhibit an efficient coupling operation together with efficient intensity modulation via the tunable permittivity of ITO. The escalation of ITO's carrier concentration during deposition at different oxygen partial pressures is used to adequately realize the ENZ zone. The electro-optical characterization of ITO deposited at zero oxygen partial pressure exhibits productive tuning of the refractive index. The lateral electro-optical coupling of depleted charge density distributed across Si-ITO vertical and horizontal heterojunctions leads to improved electrical control, providing optical modulation and tunable coupling efficiency. An extinction ratio of 24 dB for an 80- μm -long device at a maximum reverse-bias voltage of -4 V is reported with an energy consumption of 36 pJ. The structure can also be enabled as a passive coupler and a small-footprint phase shifter with 0.34 V/mm efficiency. The proposed multifunctional compact device with its energy efficiency can pave the way for cost-effective large-scale photonic integration. The proposed concept of the utilization of a subwavelength grating in the form of distributed semiconductor heterojunctions and a coupler together with electrical tuning of ITO opens avenues for a variety of integrated optoelectronic devices for future flexible optical networks, optical interconnects, and computing.

ACKNOWLEDGMENT

The authors are thankful to Dr. C. Mukherjee, Head, Optical Coatings Lab, Advanced Laser & Optics Division, RRCAT Indore for ion-assisted e -beam deposition. The authors would also like to thank the Nanoscale Research Facility, Indian Institute of Technology Delhi, for the electron-beam lithography facility. The authors acknowledge the characterization facilities of the Hybrid Nanodevice Research Group, Electrical Engineering and National Characterization Facility, Material Engineering & Material Science, IIT Indore. The authors are thankful for financial support given by Nanomission, Department of Science and Technology, Government of India through Grant No. DST/NM/NT/1009/2017(G). The authors also acknowledge financial aid from the Council of Scientific and Industrial Research, Government of India, through Grant No. 22/814/19/EMR-II and partial financial support from Oxford Instruments.

S. Rajput and M. Kumar developed the device concept and carried out theoretical analysis. S. Rajput, V. Kaushik, and P. Babu fabricated the device and carried out device measurements. P. Tiwari and A. K. Srivastava guided the partial fabrication process. M. Kumar guided the whole fabrication process and characterization. S. Rajput, V. Kaushik, P. Babu, and M. Kumar analyzed data and wrote the manuscript.

APPENDIX: DETAILS OF EXPERIMENTS AND NUMERICAL ANALYSIS

1. Numerical analysis and experimental section numerical analysis

Analysis of the laterally coupled distributed semiconductor heterojunctions for comprehensive charge transport is done by employing a three-dimensional (3D) charge-transport simulator. The charge monitor across the device is persistently solving the equations depicting electrostatic potential and the density of free carriers. The transmission characteristics and modal analysis of the Si-ITO subwavelength-grating coupler at 1550 nm, with perfectly matched layer boundary conditions, are computed by employing LUMERICAL 3D finite-difference time-domain (FDTD) solutions and the finite-difference eigenmode (FDE) solver of MODE solutions, respectively. The FDE solver calculates the modal spatial profile and frequency dependence by solving Maxwell's equations on a cross-section mesh of the waveguide. The field distributions in the gratings are monitored to attain the maximum coupling efficiency and reducing back reflections for a grating period ($\check{\text{D}}$) of 600 nm. The coupling efficiency is numerically calculated using the FDTD solver of LUMERICAL solutions. The fundamental TE mode of a wavelength of 1550 nm at an angle of 10° with respect to the normal is sourced at the top of the FDTD simulation region and propagates along with the Si-ITO gratings. The field distribution in the gratings is monitored to attain the maximum coupling efficiency and reducing back reflections for a grating period ($\check{\text{D}}$) of 600 nm. The coupled power is measured using $P_{\text{coupled}} = P_{\text{injected}} - (P_{\text{reflected}} + P_{\text{transmission}})$. The power transmission monitors are placed below and above the Si-ITO heterojunction-based grating coupler to measure the reflected and transmitted power, which is later subtracted from the injected power. Furthermore, to calculate the coupling efficiency with respect to wavelengths ranging from 1530 to 1570 nm at different reverse-bias voltages, the LUMERICAL charge-transport solver is incorporated. The LUMERICAL charge-transport solver calculates the spatial depletion of charge-carrier density holes and electrons across the distributed semiconductor heterojunctions in the Si-ITO grating coupler. The charge-carrier density at different voltages obtained from the charge solver is transported to FDTD and MODE solutions via an index perturbation (n - p density) grid, which tunes the optical constant of ITO, leading to a change in the complex effective index of the mode.

2. Deposition of ITO and electrical characterization

The ITO layer is deposited on highly doped p -type SOI wafer at three different oxygen partial pressures. The p -type Si wafers are ultrasonically cleaned and an ion-assisted e -beam deposition unit is utilized to carry out

deposition at oxygen partial pressures of (i) 1 sccm and 30 sccm Ar, (ii) 0.5 sccm and 30 sccm Ar, and (iii) 0 sccm and 30 sccm Ar using a commercially available ITO ceramic target and 99.99% pure oxygen. Inside the deposition chamber, the background and working pressures are maintained at 5.7×10^{-7} and 7.5×10^{-3} mbar, respectively, whereas the ion-beam voltage and power are kept at 190 V and 50 W, respectively. Deposition is carried out at a rate of 0.5 Å/s. After deposition, the wafers are annealed at 200 °C for 30 min. The carrier density and conductivity of the deposited ITO films are measured on a room-temperature Hall effect measurement setup with van der Pauw geometry at 0.6 T magnetic field and 1 mA current.

3. Electro-optical characterization and device processing

A J. A. Woollam M-2000 DI spectroscopic ellipsometer is employed to measure the optical constants of the deposited ITO thin films, as it can provide fast and precise thin-film characterization over a wide spectroscopic range. VASE data are extracted for three different angles of 65°, 70°, and 75°. An ITO general-oscillator model is used to fit VASE data and corresponding optical constants are found. A mean-square error value of 4.85 and uniqueness of the fitted thickness parameter coupled with thickness matching from deposition reinforces the fit.

The fabrication of the grating coupler structure starts with a standard cleaning of the *p*-type SOI wafer accompanied by spin coating of the *e*-beam resist. First, a low-weight resist (PMMA A4, wt 495 K) is spin-coated at 4500 rpm for 1 min on highly doped *p*-type SOI wafer. In the second step, PMMA A4 (wt 950 K) is spin-coated at 4500 rpm for 1 min and then the wafer is prebaked at 180 °C for 30 min. Eline Plus Raith electron-beam lithography (EBL) is utilized to transfer the pattern (Si-air grating of $\text{ED} = 600$ nm) on the resist-coated wafer. The EBL writing parameters are 10 kV accelerating voltage, 30 μm aperture, 10 mm working distance, with a dose of 100 $\mu\text{C}/\text{cm}^2$. Later, the wafer is developed for 4.5 min and is further processed for reactive-ion etching. Si is etched to a desired depth of 130 nm using 38 sccm SF_6 and 14 sccm CHF_3 at a pressure of 80 mTorr for 5 min. Once the Si-air grating structure is patterned, then ITO is deposited over it by employing ion-assisted *e*-beam deposition. Deposition is carried out under the same parameters with a partial pressure of 0 sccm O_2 and 40 sccm Ar because of the ENZ state of ITO with these parameters. To make an ohmic contact on ITO, indium is soldered and annealed under vacuum, whereas to make a good ohmic contact on Si, aluminum is deposited on Si using a metal-deposition unit at a working pressure of 4×10^{-3} mbar, a voltage of 300 V, and a current of 0.22 A in an Ar partial pressure of 40 sccm.

- [1] A. E. J. Lim, J. Song, Q. Fang, C. Li, X. Tu, N. Duan, K. K. Chen, R. P. C. Tern, and T. Y. Liow, Review of silicon photonics foundry efforts, *IEEE J. Sel. Top. Quantum Electron.* **20**, 405 (2014).
- [2] R. Won and M. Paniccia, Integrating silicon photonics, *Nat. Photon.* **4**, 498 (2010).
- [3] M. Hochberg and T. Baehr-Jones, Towards fabless silicon photonics, *Nat. Photon.* **4**, 492 (2010).
- [4] C. K. Tang and G. T. Reed, Highly efficient optical phase modulator in SOI waveguides, *Electron Lett.* **31**, 451 (1995).
- [5] A. R. Soref and B. R. Bennett, Electro-optical effects in silicon, *IEEE J. Quantum Electron.* **23**, 123 (1987).
- [6] C. E. Png, S. P. Chan, S. T. Lim, and G. T. Reed, Optical phase modulators for MHz and GHz modulation in silicon-on-insulator, *J. Lightwave Technol.* **22**, 1573 (2004).
- [7] G. T. Reed, G. Mashanovich, F. Y. Gardes, and D. J. Thomas, Silicon optical modulators, *Nat. Photon.* **4**, 518 (2010).
- [8] C. K. Tang, G. T. Reed, A. J. Walton, and A. G. Rickman, Low-Loss single mode optical phase modulator in SIMOX material, *J. Lightwave Technol.* **12**, 1394 (1994).
- [9] R. Amin, J. B. Khurgin, and V. J. Sorger, Waveguide-based electro-absorption modulator performance: Comparative analysis, *Opt. Exp.* **26**, 15445 (2018).
- [10] S. Jain, S. Rajput, V. Kaushik, Sulabh, and M. Kumar, Efficient optical modulation With high data-rate in silicon based laterally split vertical p-n junction, *IEEE J. Quant. Electron.* **56**, 1 (2020).
- [11] M. R. Watts, W. A. Zortman, D. C. Trotter, R. W. Young, and A. L. A. L. Lentine, Vertical junction silicon microdisk modulators and switches, *Opt. Exp.* **19**, 21989 (2011).
- [12] K. Shi, R. R. Haque, B. Zhao, R. Zhao, and Z. Lu, Broadband electro-optic modulator based on transparent conducting oxide, *Opt. Lett.* **39**, 4978 (2014).
- [13] Z. Zhang, B. Huang, Z. Zhang, C. Cheng, and H. Chen, Bidirectional grating coupler based optical modulator for low-loss integration and low-cost fiber packaging, *Opt. Exp.* **21**, 14202 (2013).
- [14] S. Rajput, V. Kaushik, S. Jain, and M. Kumar, Slow light enhanced PhaseShifter based on Low-loss silicon-ITO hollow waveguide, *IEEE Phot. J.* **11**, 1 (2019).
- [15] X. Liu, K. Zang, J.-H. Kang, J. Park, J. S. Harris, P. G. Kik, and M. L. Brongersma, Epsilon-near-zero Si slot-waveguide modulator, *ACS Photon.* **11**, 4484 (2018).
- [16] J. T. Kim, CMOS-compatible hybrid plasmonic modulator based on vanadium dioxide insulator-metal phase transition, *Opt. Lett.* **39**, 3997 (2014).
- [17] V. E. Babicheva, A. Boltasseva, and A. V. Lavrinenko, Transparent conducting oxides for electro-optical plasmonic modulators, *Nanophot.* **4**, 165 (2015).
- [18] L. Singh, S. Jain, and M. Kumar, Electrically writable silicon nanophotonic resistive memory with inherent stochasticity, *Opt. Lett.* **44**, 4020 (2019).
- [19] H. W. Lee, G. Papadakis, S. P. Burgos, K. Chander, A. Kriesch, R. Pala, U. Peschel, and H. A. Atwater, Nanoscale conducting oxide PlasMOSTor, *Nanolett.* **14**, 6463 (2014).

- [20] M. Liu, X. Yin, E. Ulin-Avila, B. Geng, T. Zentgraf, L. Ju, F. Wang, and X. Zhang, A graphene-based broadband optical modulator, *Nature* **474**, 64 (2011).
- [21] H. Dalir, Y. Xia, Y. Wang, and X. Zhang, Athermal broadband graphene optical modulator with 35 GHz speed, *ACS Photon.* **3**, 1564 (2016).
- [22] C. Ye, S. Khan, Z. R. Li, E. Simsek, and V. J. Sorger, λ -size ITO and graphene-based electro-optic modulators on SOI”, *IEEE J. Sel. Topics Quantum Electron.* **20**, 40 (2014).
- [23] S. Rajput, V. Kaushik, S. Jain, P. Tiwari, A. K. Srivastava, and M. Kumar, ” optical modulation in hybrid waveguide based on Si-ITO heterojunction”, *J. Lightwave Technol.* **38**, 135 (2020).
- [24] Q. Gao, E. Li, and A. X. Wang, Ultra-compact and broadband electro-absorption modulator using an epsilon near zero conductive oxide, *Phot. Res.* **6**, 277 (2018).
- [25] A. P. Vasudev, J. H. Kang, J. Park, X. Liu, and M. L. Brongersma, Electro-optical modulation of a silicon waveguide with an “epsilon-near-zero” material, *Opt. Exp.* **21**, 26387 (2013).
- [26] V. Kaushik, S. Rajput, and M. Kumar, Broadband optical modulation in zinc oxide based heterojunction via optical lifting, *Opt. Lett.* **45**, 363 (2020).
- [27] Z. Ma, Z. Li, K. Liu, C. Ye, and V. J. Sorger, Indium Tin oxide for high performance electro-optic modulation, *Nanophot.* **4**, 198 (2016).
- [28] M. Z. Alam, I. D. Leon, and R. W. Boyd, Large optical Non-linearity of indium Tin oxide in its epsilon near zero region, *Nonlinear Optics* **352**, 795 (2016).
- [29] M. K. Shah, R. Lu, and Y. Liu, Enhanced performance of ITO-assisted electro-absorption optical modulator using sidewall angled silicon waveguide, *IEEE Trans. on Nanotech.* **17**, 412 (2018).
- [30] J. Baek, J. B. You, and K. Yu, Free-carrier electro-refraction modulation based on a silicon slot waveguide with ITO, *Opt. Exp.* **23**, 15863 (2015).
- [31] H. Zhao, Y. Wang, A. Capretti, L. D. Negro, and J. Klamklin, Broadband electro-absorption modulators design based on epsilon-near-zero indium Tin oxide, *IEEE J. Sel. Topics Quantum Electron.* **21**, 3300207 (2015).
- [32] W. Jiang, J. Miao, and T. Li, Silicon mode-selective switch via horizontal metal-oxide-semiconductor capacitor incorporated With ENZ-ITO, *Scient. Rep.* **9**, 1 (2019).
- [33] E. Feigenbaum, K. Diest, and H. A. Atwater, Unity- order index change in transparent conducting oxides at visible frequencies, *Nano Lett.* **10**, 2111 (2010).
- [34] R. Amin, C. Suer, Z. Ma, I. Sarpkaya, J. B. Khurgin, R. Agarwal, and V. J. Sorger, Active material, optical mode and cavity impact on nanoscale electro-optic modulation performance, *Nanophot.* **7**, 455 (2017).
- [35] R. Amin, R. Maiti, C. Carfano, Z. Ma, M. H. Tahersima, Y. Lilach, D. Ratnayake, H. Dalir, and V. Sorger, 0.52V-mm ITO-based mach-zehnder modulator in silicon photonics, *APL Photon.* **3**, 126104 (2018).
- [36] C. Dealcour, S. Blaize, P. Grosse, J. M. Fedeli, A. Bruyant, R. Salas-Montiel, G. Lerondel, and A. Chelnokov, Efficient directional coupling between silicon and copper plasmonic nanoslot waveguides: Toward metal-oxide-silicon nanophotonics, *Nano Lett.* **10**, 2922 (2010).
- [37] M. Lipson, Guiding, modulating, and emitting light on silicon-challenges and opportunities, *J. Lightwav. Technol.* **23**, 4222 (2005).
- [38] J. S. Kim and J. T. Kim, Silicon electro-optic modulator based on an ITO-integrated tunable directional coupler, *J. Phys. D: Appl. Phys.* **49**, 075101 (2016).
- [39] Z. Wag, X. Xu, D. Fan, Y. Wang, H. Subbaraman, and R. T. Chen, Geometrical tuning art for entirely subwavelength grating waveguide based integrated photonics circuits, *Scient. Rep.* **6**, 24106 (2016).
- [40] S. Jain, Sulabh, S. Rajput, L. Singh, P. Tiwari, A. Srivastava, and M. Kumar, Thermally stable optical filtering using silicon-based comb-like asymmetric grating for sensing applications, *IEEE Sensors J.* **20**, 3529 (2019).
- [41] P. Cheben, R. Halir, J. H. Schmid, H. A. Atwater, and D. R. Smith, Subwavelength integrated photonics”, *Nature* **560**, 565 (2018).
- [42] P. J. Bock, P. Cheben, J. H. Schmid, J. Lapointe, A. Delage, S. Janz, G. C. Aers, D. X. Xu, A. Densmore, and T. J. Hall, Subwavelength grating periodic structures in silicon-insulator: A new type of microphotonic waveguide, *Opt. Exp.* **18**, 20251 (2010).
- [43] C. L. Tien, H. Y. Lin, C. K. Chang, and C. J. Tnag, Effect of oxygen flow rate on the optical, electrical and mechanical properties of DC sputtering ITO thin films, *Hindawi Adv. in Cond. Matt. Phys.* **11**, 1 (2018).
- [44] M. Bender, W. Seelig, C. Daube, H. Frankenberger, B. Ocker, and J. Stollenwerk, Dependence of oxygen flow on optical and electrical properties, *Thin Solid Films* **326**, 72 (1998).
- [45] L. J. Meng and M. P. Dos Santos, Structure effect on electrical properties of ITO films prepared by RF reactive magnetron sputtering, *Thin Solid Films* **289**, 65 (1996).
- [46] V. Kaushik, S. Rajput, S. Shrivastava, S. Jain, L. Singh, and M. Kumar, Efficient Sub-bandgap photodetection via Two-dimensional electron Gas in ZnO based heterojunction, *J. Lightwave Technol.* **38**, 6031 (2020).
- [47] L. Kerkache, A. Layadi, and A. Mosser, Effect of oxygen partial pressure on the structural and optical properties of DC sputtered ITO thin films, *J. Alloys and Compd.* **2009**, 46 (2009).
- [48] J. Bregman and Y. Shapira, Effects of oxygen partial pressure during deposition on the properties of Ion-beam sputtered indium-tin-oxide thin films, *J. App. Phys.* **67**, 3750 (1990).
- [49] C. Wang, M. Zhang, B. Stern, M. Lipson, and M. Loncar, Nanophotonic lithium niobate electro-optic modulators, *Opt. Exp.* **26**, 1547 (2018).
- [50] M. Streshinsky, R. Ding, Y. Liu, A. Novack, Y. Yang, Y. Ma, X. Tu, E. K. S. Chee, A. E.-J. Lim, P. G.-Q. Lo, T. Baehr-Jones, and M. Hochberg, Low power 50Gbps silicon travelling wave mach-zehnder modulator near 1300nm”, *Opt. Exp.* **21**, 030350 (2013).
- [51] M. Liu, X. Yin, and X. Zhang, Double-layer graphene optical modulator”, *Nano Lett.* **12**, 1482 (2012).
- [52] V. J. Sorger, N. D. Lanzillotti-Kimura, R. M. Ma, and X. Zhang, Ultracompact silicon nanophotonic modulator with broadband response, *Nanophot.* **1**, 17 (2012).